CHAPTER III
SYNTHESIS OF MAGNETIC NANOPARTICLE INTO BACTERIAL CELLULOSE MATRIX BY AMMONIA GAS-ENHANCEING *IN SITU* CO-PRECIPITATION METHOD

3.1 Abstract

In this study, magnetically responsive bacterial cellulose sheets were prepared by using an ammonia gas-enhancing *in situ* co-precipitation method operated in a closed system without oxygen. Instead of using the traditional concentrated liquid basic solutions, ammonia gas was used in the closed system to achieve the homogeneous dispersion of magnetic nanoparticles as evidence by the uniform black color of magnetic nanoparticles across the cross-sectional area of bacterial cellulose sheets. In addition, under the condition without oxygen, the synthesized magnetic would be in the form of magnetite (Fe_3O_4). The formation of magnetic nanoparticles inside bacterial cellulose sheets was investigated by scanning electron microscopy (SEM), X-ray diffraction (XRD), and energy dispersive X-ray (EDX). The average particle size of the magnetic nanoparticles was determined by using transmission electron microscopy (TEM) and was found to be in the ranged of 19.6 to 38.9 nm. The homogeneous dispersion of magnetic nanoparticles across the cross-sectional area of the bacterial cellulose samples was also evidenced by SEM and TEM images. Moreover, the magnetic field responsive behavior of the magnetic nanoparticle-incorporated bacterial cellulose sheets was investigated by vibrating sample magnetometry (VSM). The saturation magnetization of the magnetic nanoparticle-incorporated bacterial cellulose sheets ranged from 1.92 to 26.20 emu/g at 300 K and ranged from 2.96 to 28.10 emu/g at 100 K.

3.2 Introduction

Magnetically responsive materials are specific subsets of smart materials, in which magnetic nanoparticles are embedded in a polymer matrix, which can adaptively change their physical properties due to an external magnetic field

interesting magnetic field-dependent mechanical behavior with a wide range of potential applications such as fibers and fabrics for protective clothing for military use (Raymond *et al.*, 1994), magnetic filters (Pinchuk *et al.*, 1995), sensors (Epstein & Miller, 1996), information storage, static and low frequency magnetic shielding (Dikeakos *et al.*, 2003) and health care or biomedical products (Wang *et al.*, 2004). In general, magnetically responsive materials consist of two main compositions which are magnetic nanoparticles and polymer matrix such as magnetic nanoparticles/cellulose (Small & Johnston, 2009), magnetic nanoparticles/poly(acrylonitrile-co-acrylic acid) (Guo *et al.*, 2009), magnetic nanoparticles/poly(vinyl chloride) (Rodriguez-Fernandez *et al.*, 2008), magnetic nanoparticles/poly(methyl methacrylate) (Baker *et al.*, 2004), magnetic nanoparticles /poly(aniline) (Shchukin, Radtchenko, & Sukhorukov, 2003), magnetic nanoparticles /poly(acrylamide) (Starodoubtsev *et al.*, 2003).

Magnetic nanoparticles are nanoparticles of iron oxides. In nature, iron oxides exist in various forms including hematite (α-Fe_2O_3), maghemite (γ-Fe_2O_3) and magnetite (Fe_3O_4) (Cornell & Schwertmann, 2003). Hematite is blood-red iron oxide. It is the oldest known iron oxide and often is the end product of the transformation of other forms of iron oxides at ambient conditions (Teja & Koh, 2009). Maghemite is a metastable state of iron oxide. It is formed by weathering or low-temperature oxidation of magnetite (Majewski & Thierry, 2007). Magnetite is a black iron oxide. It exhibits the strongest magnetism of any transition metal oxides (Cornell & Schwertmann, 2003; Majewski & Thierry, 2007). It has been reported that, magnetite exhibits biocompatibility and low toxicity in human body (Majewski & Thierry, 2007; Tartaj *et al.*, 2003; Kim *et al.*, 2005; Tartaj *et al.*, 2005).

Lower than approximately 100 nm in diameter, particles of ferromagnetic materials, which are materials that exhibit permanent magnetization even with or without magnetic field, no longer exhibit the ferromagnetic behavior which is found in the bulk. Instead, such nanoparticles exhibit superparamagnetic behavior which no longer exhibits a history-dependent behavior or hysteresis (Wang *et al.*, 2004). The superparamagnetic materials are different from permanent magnet in that the magnetic interactions of nanoparticles of iron oxide are induced by external magnetic field while without external magnetic field, nanoparticles of iron oxide no longer

show magnetic interaction (Neuberger *et al.*, 2005). Accordingly, there are two main requirements for preparing magnetically responsive materials which are the as-synthesized iron oxide particles should be in the form of magnetite and the diameter of the as-synthesized iron oxide particles should be lower than 100 nm (Wang *et al.*, 2004).

Bacterial cellulose belongs to a specific product of primary metabolism of the acetic bacterium such as *Acetobacter xylinum*. Bacterial cellulose is synthesized in the form of fibrous structure which constitutes to be a three-dimensional non-woven network of nanofibers with diameters less than 100 nm, which is much smaller than the diameters of typical plant cellulose bundles (ca. 10 μm). Bacterial cellulose has the same chemical structure as plant cellulose (Czaja, Romanovicz, & Brown, 2004). The presence of inter- and intra-hydrogen bonding in bacterial cellulose results in the never dried-state material or hydrogel having high wet strength (Meftahi *et al.*, 2010). One of the most important features of bacterial cellulose is its chemical purity. Bacterial cellulose is free of lignin and hemicellulose, whereas plant cellulose usually associates with these chemicals. Owing to these unique properties, bacterial cellulose is an interesting material for using in wide range of applications such as paper industrial, headphone membrane, food industrial (Li *et al.*, 2009), biomaterials including temporary skin substitute, artificial blood vessels (Czaja *et al.*, 2007; Kamel, 2007), membrane for pervaporation of water-ethanol binary mixtures (Dubey *et al.*, 2002) and an applicable matrix for impregnating nanoparticles or nanowires (Zhang & Qi, 2005; Maneerung, Tokura, & Rujiravanit, 2008; Hu *et al.*, 2009; Li *et al.*, 2009; Hu *et al.*, 2010). In addition, bacterial cellulose has unique micro-porous three-dimensional network structure and high specific surface area (Hu *et al.*, 2010). The high specific surface area implies that bacterial cellulose has much more surface hydroxyl and ether groups than plant cellulose. These hydroxyl groups make up of active sites for metal ion adsorption (Li *et al.*, 2009). Moreover, the porous structure of nanofibrous bacterial cellulose provides large amount of sub-micron pores. The precipitated metal nanoparticles are stabilized by the sub-micron pores of the bacterial cellulose, leading to good dispersion of the as-synthesized nanoparticles (Hu *et al.*, 2009). Therefore, bacterial cellulose is considered as a promising matrix for synthesizing of nanoparticles and

nanowires such as ZnO nanoparticles (Hu *et al.*, 2010), CdS nanoparticles (Li *et al.*, 2009), silver chloride nanoparticles (Hu *et al.*, 2009), silver nanoparticles (Maneerung, Tokura, & Rujiravanit, 2008) and titania (anatase) nanowires (Zhang & Qi, 2005).

The preparation of magnetically responsive materials based on cellulose and magnetic nanoparticles has been investigated by several approaches. In the past 2 to 3 decades, magnetically responsive cellulose fibers have been prepared by vigorously agitation of cellulose pulp in a concentrated suspension of iron oxide particles such as magnetite particles and maghemite particles, followed by a mild washing step to remove all unbound-magnetic particles. This preparation method is called lumen-loading method (Green, Fox, & Scallan, 1982; Marchessault, Rioux, & Raymond, 1992; Passaretti, Caulfield, & Sobczynskyi, 1990; Rioux, Ricard, & Marchessault, 1992). The percentage loading of the iron oxide particles was limited by the low diffusion rate of iron oxide particles into cellulose pulp. The as-prepared products from the lumen-loaded method were exhibited the magnetic hysteresis loop being comparable to those observed in the magnetic strip (Raymond *et al.*, 1994). Another approach to prepare magnetically responsive cellulose fibers involves synthesizing of iron oxide particles within the cellulosic matrix itself by vigorously agitation of cellulose pulp in iron ion solution and then iron ions are converted to iron oxide particles within cellulosic matrix by the addition of an excess NaOH solution. This preparation method was called *in situ* co-precipitation method (Marchessault, Richard, & Rioux, 1992; Marchessault, Rioux, & Raymond, 1992). According to the literature, the *in situ* co-precipitation method offers better control of both the magnetic properties and the variety of magnetic particles that are incorporated into the final product than the lumen-loaded method (Small & Johnston, 2009). Sourty, Ryan, and Marcessault (1998) prepared magnetically responsive bacterial cellulose membranes by stepwise dipping process. Bacterial cellulose pellicles were firstly dipped in a solution of $FeCl_2 \cdot 4H_2O$, followed by dipping in a fresh solution of NaOH. The suspension was then heated in a water bath at 65 °C, followed by adding hydrogen peroxide. Finally, samples were washed against distilled water. This method was a modification of *in situ* co-precipitation method by dipping bacterial cellulose into the individual reagents rather than immersed in a single container. By

this mean the individual reaction was exclusively occurred step by step inside bacterial cellulose. However, this stepwise dipping process still had some drawbacks. The obtained samples showed the un-uniform dispersion of the precipitated nanoparticles across the cross-sectional area of bacterial cellulose. Formation of the darker skin at the surface resulted from the predominant forming of ferrites at the surface of the processed bacterial cellulose. Moreover, the dipping process was done under ambient condition. As a result, the present of oxygen gas in the atmospheric air promotes the formation of maghemite (γ-Fe_2O_3) and hematite (α-Fe_2O_3). These two products exhibit weaker magnetic property than magnetite (Fe_3O_4) (Teja & Koh, 2009), resulting in lower saturation magnetization.

In this study, magnetic nanoparticles were synthesized inside the porous structure of bacterial cellulose by using the ammonia gas-enhancing *in situ* co-precipitation method operated in the closed system as shown in the schematic diagram of the experimental set up (Figure 3.1). The utilization of ammonia gas could achieve the homogeneous dispersion of the magnetic nanoparticles across the cross-sectional area of the as-synthesized sample since ammonia gas more easily penetrates through the porous structure of bacterial cellulose. In addition, the utilization of ammonia gas could slightly increase the pH of the as-synthesized sample. This could eliminate the high local concentration of liquid basic solution at surface of the processed bacterial cellulose which is the cause of predominantly forming of ferrites at the surface of bacterial cellulose. Moreover, the utilization of ammonia gas treatment was conducted in the closed system which could eliminate the oxygen gas by previously flushing with nitrogen gas. In the absence of oxygen gas, the predominant form of magnetic nanoparticles inside bacterial cellulose is magnetite which exhibited the highest saturation magnetization.

3.3 Experimental

3.3.1 Materials

Acetobacter xylinum (strain TISTR 975), an isolated strain in Thailand, was supplied from the Microbiological Resources Centre, Thailand Institute of Scientific and Technological Research (TISTR). Analytical grade of

anhydrous D-glucose was obtained from Ajax Finechem. Bacteriological grade of yeast extract powder was purchased from HiMedia. Analytical grade ferric chloride ($FeCl_3 \cdot 6H_2O$) and ferrous sulphate ($FeSO_4 \cdot 7H_2O$) were purchased from Riedel-deHaën and Ajax Finechem, respectively. Other chemical reagents used in this study were analytical grade and used without further purification.

3.3.2 *Production of bacterial cellulose*

The production of the bacterial cellulose pellicles were performed by a partial modification of the method developed by Maneerung, Tokura, and Rujiravanit (2008).

The pre-inocula for all experiments were prepared by transferring a single colony of *Acetobacter xylinum* (strain TISTR 975) into 20 ml of a liquid culture medium, which was composed of 40 g of anhydrous D-glucose, 10 g of yeast extract powder, and 1 l of distilled water. After 24 h of cultivation at 30 °C, 40 ml of the cell suspension was introduced into a container containing 400 ml of a fresh liquid culture medium and then cultivated at 30 °C for 4 days. The obtained bacterial cellulose was purified by boiling in 1% NaOH for 2 h. The boiling step was repeated twice. The purified bacterial cellulose was then treated with 1.5% acetic acid solution for 30 min, and finally washed in a tap water until bacterial cellulose pellicles became neutral. The purified bacterial cellulose was cut into a rectangular shape with 4 cm width and 10 cm length. The porous structure of bacterial cellulose was preserved by immersing into the distilled water and kept into a refrigerator at 4 °C prior to use.

3.3.3 *Ammonia gas-enhancing in situ co-precipitation of magnetic nanoparticles into bacterial cellulose pellicles*

Magnetic nanoparticles were synthesized into the bacterial cellulose pellicles by immersing the bacterial cellulose pellicles (ca. 99.5% water content) in an aqueous iron salt solution at 60 °C. The aqueous iron salt solution contained $FeCl_3$ and $FeSO_4$ with the mole ratio of the Fe^{3+} to Fe^{2+} ions to be fixed at 2:1. The total concentration of aqueous iron ion was varied to be 0.1 M, 0.05 M, and 0.01 M. After immersion of the bacterial cellulose pellicles into the iron salt solution for 1 h, the

excess iron, yellowish-brown particles, on the surface of the bacterial cellulose pellicles was rinsed with distilled water. After washing, the iron ion-absorbed bacterial cellulose pellicles were kept inside 500 ml wide-neck round bottom flask (a reaction vessel) and pre-treated with nitrogen gas for 10 min in order to eliminate oxygen gas before further treating with ammonia gas. The volumetric flow rate of ammonia gas was controlled by a flow meter. When ammonia gas was purged into the reaction vessel, the color of iron ion-saturated bacterial cellulose pellicles was gradually changed. After 30 min of ammonia gas treatment, the as-prepared bacterial celluloses had dark brown color. The obtained bacterial cellulose pellicles were rinsed with a large amount of distilled water until neutral and then sonicated for 20 min in order to remove any loosely bound particles. Finally, the obtained samples were freeze dried and kept in a desicator.

3.3.4 Characterization

The morphology of the neat and magnetic particle-incorporated bacterial cellulose sheets were observed by using a JEOL JSM-5200 scanning electron microscope with inbuilt energy dispersive X-ray analysis (EDX) with operating condition at 15 kV and magnification of 10,000x. The formation of magnetic particles was verified by X-ray diffraction (XRD) (Rigaku). The samples were scanned from $2\theta = 10°$ to $2\theta = 70°$ at a scanning rate of 5° 2θ/min. Thermogravimetric analyser (Perkin Elmer model TGA7) was used to record the thermograms in the temperature range from 50 to 700 °C with a heating rate of 10 °C/min in a flow of nitrogen at 20 ml/min. Transmission electron microscopy (TEM) observations were carried out on a JEOL JEM-2000EX instrument operated at accelerating voltage of 80 kv. The TEM samples were prepared by embedding the freeze dried bacterial cellulose in Spurr resin and performing ultrathin sectioning with a Reichert Ultracut E microtome equipped with a diamond knife. Histograms, average diameters and standard deviations were obtained by sampling 200 metal nanoparticles in TEM images of 100,000x magnification.

3.3.5 Vibrating sample magnetometry (VSM)

The responsiveness to the magnetic field of the magnetic particle-incorporated bacterial cellulose sheets was detected by vibrating sample magnetometer. Sample was inserted into a sample holder and vibrated within a magnetic field of up to 10,000 G. The magnetic moments of the as-prepared sample were recorded as a function of applied field at the temperatures of 300 K and 100 K and the results were reported in term of a magnetic hysteresis loop (Jiles, 1991).

3.3.6 Magnetic field responsiveness testing

A rectangular strip (length×width×thickness = 45×5×0.04 mm) of the magnetic particle-incorporated bacterial cellulose sheet was placed onto the surface of an aluminum plate with one end fixed by taping it onto the aluminum plate surface. A cylinder shaped permanent magnet was hanged above the test sample. The magnet responsive behavior of the magnetic particle-incorporated bacterial cellulose sheet was recorded by a digital camera. (Wang *et al.*, 2004)

3.4 Results and Discussion

For a comparison, the magnetic particle-incorporated bacterial cellulose pellicles were also prepared by the step-wise dipping process according to the method of Sourty, Ryan, and Marcessault (1998) and digital images of the obtained products are shown in Figures 3.2a, 3.2b and 3.2c. Briefly, bacterial cellulose pellicles were firstly dipped in an aqueous iron salt solution contained $FeCl_3$ and $FeSO_4$ with the mole ratio of the Fe^{3+} to Fe^{2+} ions of 2 to 1, followed by dipping in a fresh solution of 30% ammonia solution. The total concentrations of aqueous iron ion were varied to be 0.01 M (Figure 3.2a), 0.05 M (Figure 3.2b), and 0.1 M (Figure 3.2c). The obtained bacterial cellulose pellicles showed the darker skin at the surface which resulted from the predominant precipitation of magnetic particles at the surface of the bacterial cellulose pellicles. On the other hand, the magnetic particle-incorporated bacterial cellulose pellicles prepared by ammonia gas-enhanced *in situ* co-precipitation method had homogeneous dark color of magnetic particles across the cross-sectional area of the sample as shown in Figures 3.2d, 3.2e and 3.2f. The

colors of magnetic particles in the bacterial cellulose pellicles changed from yellow to dark brown and black when the total concentrations of aqueous iron ion were increased from 0.01 M (Figure 3.2d) to 0.05 M (Figure 3.2e) and 0.1 M (Figure 3.2f). The homogeneous dark color across the cross-sectional area of the sample implied the homogeneous dispersion of the precipitated magnetite particles across the cross-section area of bacterial cellulose pellicles.

The use of ammonia gas instead of a concentrated liquid basic solution could improve the homogeneous dispersion of the magnetic particles across the cross-sectional area of the as-synthesized bacterial cellulose pellicles since the ammonia gas is easier to penetrate through the bacterial cellulose pellicles than using concentrated liquid basic solutions. Moreover, ammonia gas could slightly increase pH of the sample and prevent the predominant precipitation of magnetic particles at the surface of bacterial cellulose pellicles.

3.4.1 Ammonia gas-enhancing in situ co-precipitation of magnetic particles into bacterial cellulose pellicles

The structure of bacterial cellulose pellicles is a three-dimensional nonwoven network consisting of a large amount of microporous. The nanofibrous structure of bacterial cellulose pellicles can serve as a support for incorporating the as-synthesized magnetic particles into bacterial cellulose pellicles. When bacterial cellulose pellicle was immersed in an aqueous iron solution, iron ions (Fe^{2+} and Fe^{3+}) could readily penetrate to the inner part of the bacterial cellulose pellicle through its porous structure. After that the bacterial cellulose pellicle was treated with ammonia gas, the absorbed Fe^{2+} and Fe^{3+} ions were precipitated to be magnetite particles into the bacterial cellulose pellicles. Finally, the lyophilize technique was used to preserve the porous structure of the bacterial cellulose.

XRD was used to examine the crystal structure of the magnetic particles. XRD analysis of the magnetic particle-incorporated bacterial cellulose sheet was performed to determine the chemical state of the iron oxide after being incorporated into the bacterial cellulose. Figure 3.3 shows the characteristic diffraction peaks of the magnetic particle-incorporated-bacterial cellulose sheet, which was prepared by using 0.1 M aqueous iron ion solution. The XRD pattern

composed of six main peaks. The peaks at 2θ = 30.40°, 35.81°, 43.53°, 54.02°, 57.59° and 63.25° corresponded to (220), (311), (400), (422), (511), and (440) planes, respectively (Guo *et al.*, 2009). These results identified the face-centered cubic (fcc) structure of the magnetite (Fe_3O_4) incorporated in the bacterial cellulose whereas the iron oxides in bacterial cellulose membranes prepared by step wise-dipping process have been reported to be were maghemite and feroxyhite (Sourty, Ryan, & Marcessault, 1998). In this study, the synthesis of magnetic particles was performed in the closed system without oxygen. Therefore, almost of the as-synthesized magnetic particles were occurred in the form of magnetite (Fe_3O_4). In comparison between magnetite and the other forms of iron oxide such as hematite (α-Fe_2O_3) and maghemite (γ-Fe_2O_3), the magnetite form (Fe_3O_4) exhibits the strongest magnetism of any transition metal oxides (Cornell & Schwertmann, 2003; Majewski & Thierry, 2007). Additionally, magnetite particles (Fe_3O_4) exhibit biocompatibility and low toxicity in human body (Majewski & Thierry, 2007; Tartaj *et al.*, 2003; Kim *et al.*, 2005; Tartaj *et al.*, 2005).

3.4.2 Morphology of magnetic particle-incorporated bacterial cellulose

The morphology of neat bacterial cellulose and bacterial cellulose incorporated with magnetite particles (Fe_3O_4) prepared by ammonia gas-enhanced *in situ* co-precipitation method were investigated by SEM analysis. Figures 3.4a and 3.4c show the surface morphology of neat bacterial cellulose and bacterial cellulose incorporated with magnetite particles (Fe_3O_4), respectively. Whereas, the cross-sectional morphology of neat bacterial cellulose and bacterial cellulose incorporated with magnetite particles (Fe_3O_4) are shown in Figures 3.4b and 3.4d, respectively. The porous structure with three-dimensional non-woven network of nanofibers which are highly un-axially oriented (Figures 3.4a and 3.4c) was observed on the surface of bacterial cellulose sheet. Whereas the multilayer of bacterial cellulose membranes linked together with the nanofibers was observed in the cross-sectional morphology of bacterial cellulose (Figures 3.4b and 3.4d). There was no change in three-dimensional network structure of bacterial cellulose after incorporation of magnetic particles by using ammonia gas-enhancing *in situ* co-precipitation method. It was also found that the use of ammonia gas could prevent the predominant

forming of magnetic particles at the surface of the processed bacterial cellulose. In addition, the magnetic particles were precipitated along the fiber surface and throughout the cross-sectional area of the processed bacterial cellulose (Figures 3.4c and 3.4d). The fiber diameters of the neat bacterial cellulose and the magnetic particle-incorporated bacterial cellulose were 55.00 ± 10.54 nm and 111.8 ± 25.79 nm, respectively. The increase in the fiber diameter of the magnetic particle-incorporated bacterial cellulose might be due to the coating of magnetic particles along the surface of bacterial cellulose fiber. The magnetic particles exhibit the potential to bond with the surface of bacterial cellulose fiber through hydrogen bonding between the oxygen in the magnetite (Fe_3O_4) and the hydrogen in the hydroxyl groups present in bacterial cellulose (Small & Johnston, 2009).

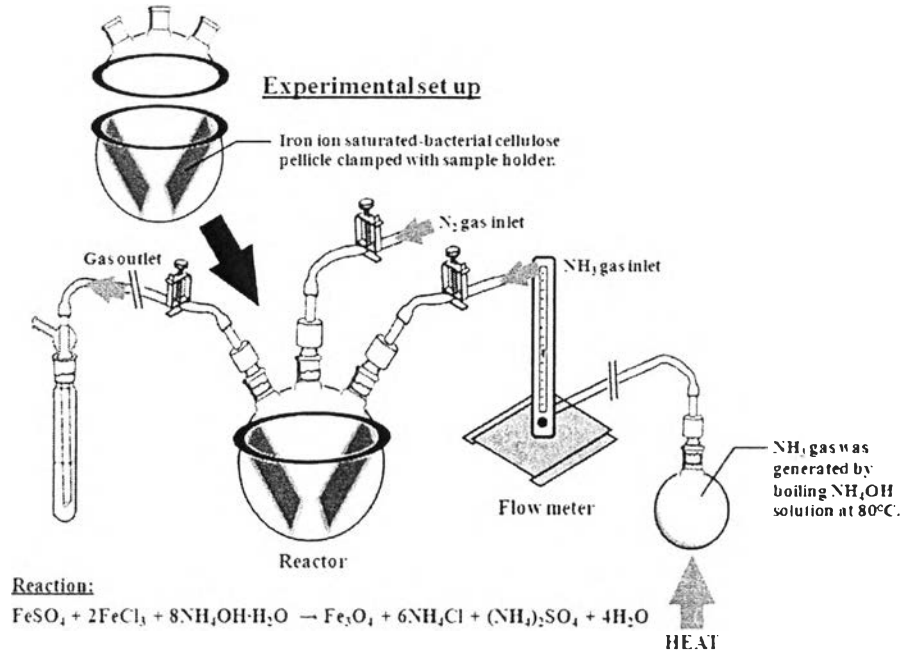

Figure 3.1 Schematic diagram of the laboratory set up for preparation of the magnetic particle-incorporated bacterial cellulose pellicle by ammonia gas-enhanced *in situ* co-precipitation method.

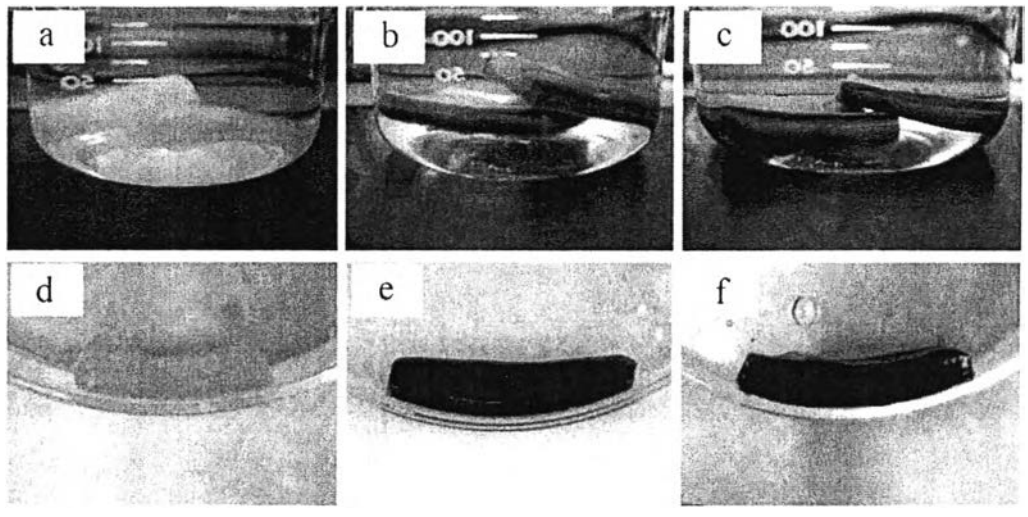

Figure 3.2 Magnetic particle-incorporated bacterial cellulose pellicles prepared by stepwise dipping process using 0.01 M (a), 0.05 M (b) and 0.1 M (c) of aqueous iron ion solutions and magnetic particle-incorporated bacterial cellulose pellicles prepared by ammonia gas-enhancing *in situ* co-precipitation method using 0.01 M (d), 0.05 M (e) and 0.1 M (f) of aqueous iron ion solutions.

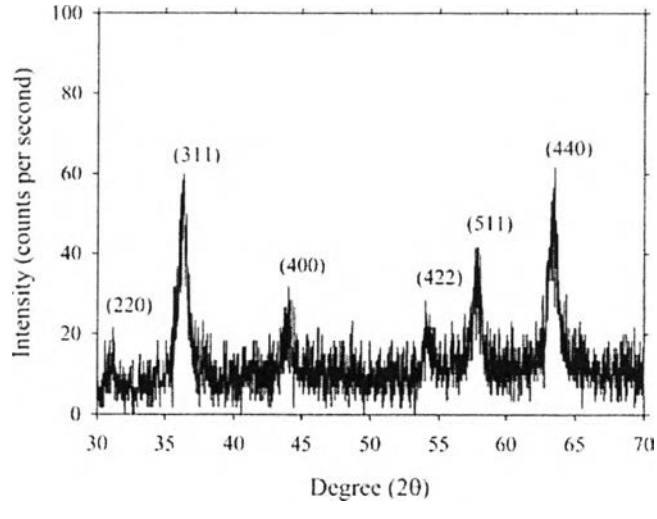

Figure 3.3 XRD pattern of magnetic particle-incorporated bacterial cellulose sheet, prepared by ammonia gas-enhanced *in situ* co-precipitation method operated in a closed system without oxygen using 0.1 M of aqueous iron ion solution.

3.4.3 *Particle size and particle size distribution of magnetic particles incorporated in bacterial cellulose sheets*

TEM microscopy was used to determine the particle size and particle size distribution of magnetite particles (Fe_3O_4) throughout the cross sections of the magnetic particle-incorporated bacterial cellulose sheets. Figure 3.5 shows the TEM micrographs of cross sections of the freeze-dried magnetic particle-incorporated bacterial cellulose sheets prepared by ammonia gas-enhancing *in situ* co-precipitation method using 0.1 M (Figure 3.5a), 0.05 M (Figure 3.5c) and 0.01 M (Figure 3.5e) of aqueous iron ion solutions. Figures 3.5a and 3.5b show the irregular shapes of the magnetic particles. The mean average particle size (d) and standard deviations (σ) of magnetite particles (Fe_3O_4) prepared by using 0.1 M aqueous iron ion solutions were estimated to be 38.92 and 10.50 nm, respectively. When the concentration of the aqueous iron ion solution was decreased from 0.1 to 0.05 M, the average particle size and particle size distribution (σ) were decreased to 32.48 and 9.71 nm, respectively (Figure 3.5c and 3.5d). At the 0.01 M aqueous iron ion solution, the well dispersed and regular shaped magnetite nanoparticles (Fe_3O_4) were obtained. The particle size was much smaller (d = 19.62 nm) and the size distribution became narrower (σ = 7.23 nm) than those obtained at higher iron concentrations, as shown in Figures 3.5e and 3.5f. The decrease in the particle size with decreasing concentration of the aqueous iron ion solution has been reported in the literature (Small & Johnston, 2009; Deepa *et al.*, 2004). Therefore, the particle size and particle size distribution of the magnetic particles could be controlled by adjusting the concentration of the aqueous iron ion solution. Small and Johnston (2009) prepared magnetically responsive cellulose fiber by using the Kraft pulp as a matrix. The average fiber diameter of the Kraft pulp was approximately 20 μm. The particle sizes of magnetic nanoparticle prepared by using the Kraft pulp as a matrix were approximately 100 nm whereas the as synthesized magnetic particle prepared by using bacterial cellulose as a matrix were ranged from 19.62 to 38.92 nm. This revealed the merit of bacterial cellulose as a matrix. Sourty, Ryan, and Marcessault (1998) prepared magnetically responsive bacterial cellulose membrane by using step wise dipping process. The synthesis of magnetic particles was performed by using 0.05 M $FeCl_2 \cdot 4H_2O$ solution and the dipping process were repeated for 3 cycles. The particle

sizes of magnetic particle prepared by the 3-cycles stepwise dipping process were approximately 50 nm whereas in this study, the average particle size of the magnetic particle prepared by ammonia gas-enhancing *in situ* co-precipitation method were 32.48 ± 9.71nm. The smaller particle size of magnetic particle resulted in the higher superparamagnetic behavior of the magnetically responsive bacterial cellulose sheets (Cornell & Schwertmann, 1996).

Moreover, the distribution of magnetic particles across the cross-sectional area of bacterial cellulose sheet was investigated by TEM analysis. TEM micrograph of cross sections of the freeze-dried magnetic particle-incorporated bacterial cellulose sheet is shown in Figure 3.6. The multilayer of the aligned magnetic particles can be observed. This implied that the magnetic particles were precipitated on the surface of bacterial cellulose fiber. The distance between the layers of the aligned magnetic nanoparticles also corresponded to the distance between the layers of neat bacterial cellulose.

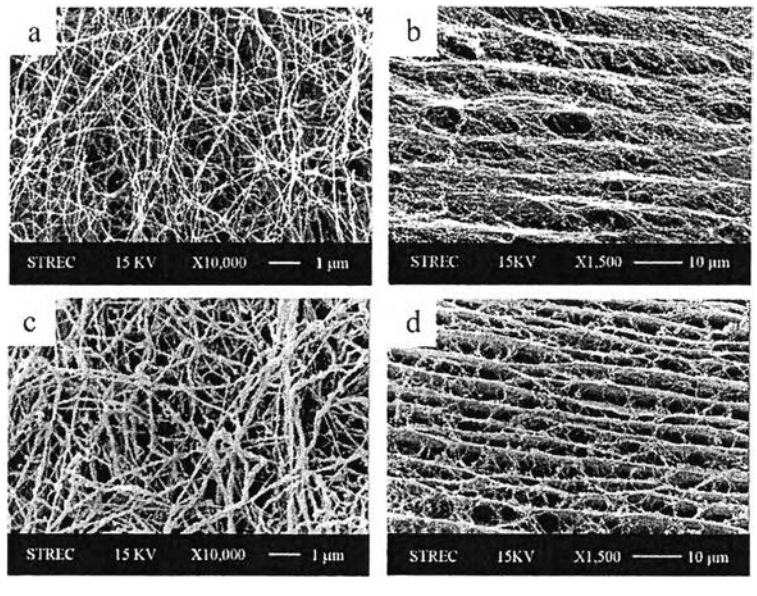

Figure 3.4 SEM images of surface (a) and cross-sectional (b) morphology of neat bacterial cellulose at a magnification of 10,000x and SEM images of surface (c) and cross-sectional (d) morphology of magnetic particle-incorporated bacterial cellulose sheet prepared by ammonia gas-enhanced *in situ* co-precipitation method using 0.1 M of aqueous iron ion solution at a magnification of 10,000x.

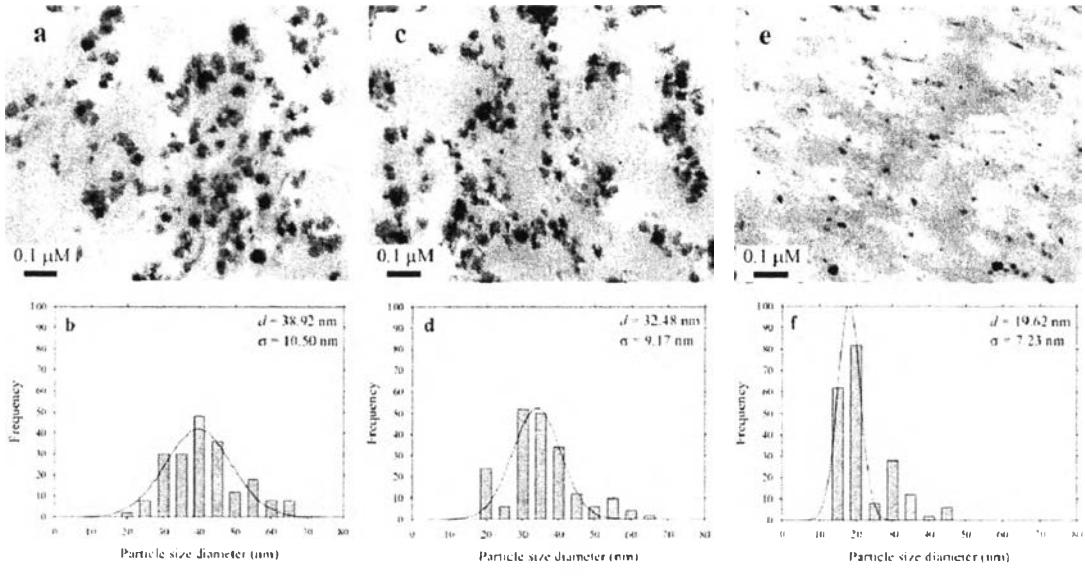

Figure 3.5 TEM images and histograms of magnetic particle-incorporated bacterial cellulose sheet prepared by ammonia gas-enhanced *in situ* co-precipitation method using 0.1 M (a and b), 0.05 M (c and d), and 0.01 M (e and f) of aqueous iron ion solution.

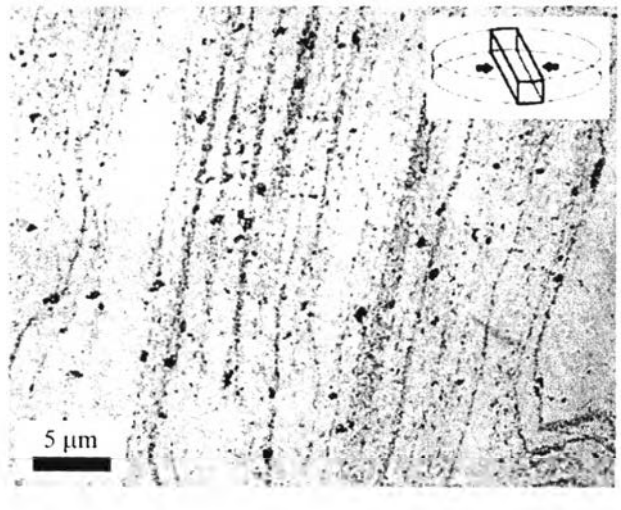

Figure 3.6 TEM image of cross-sectional magnetic particle-incorporated bacterial cellulose sheet at a magnification of 2,500×.

3.4.4 *Magnetically responsive behavior of the freeze-dried magnetic particle-incorporated bacterial cellulose sheets*

The magnetically responsive behavior of the freeze-dried magnetic particle-incorporated bacterial cellulose sheets were determined by using vibrating sample magnetometry (VSM). The hysteresis loops of the magnetic particle-incorporated bacterial cellulose sheets at the temperatures of 300 K and 100 K are shown in Figures 3.7a and 3.7b, respectively. Figures 3.7c and 3.7d show the magnified view of the corresponding loops at the temperatures of 300 K and 100 K, respectively. The dependence of the magnetization (M) with the applied magnetic field (H) is described by the Langevin equation (Cornell & Schwertmann, 1996):

$$M = M_s (\coth y - 1/y),$$

where M_s is the saturation magnetization and $y = mH/k_BT$. (m is the average magnetic moment of an individual particle in the sample, k_B is the Boltzmann constant and T is temperature).

At the temperature of 300 K, the saturation magnetizations of the magnetic particle-incorporated bacterial cellulose sheets prepared by ammonia gas-enhanced *in situ* co-precipitation method using 0.1 M, 0.05 M and 0.01 M aqueous iron ion solutions were 26.20 emu/g, 15.85 emu/g and 1.92 emu/g, respectively (Figure 3.7a). When the temperature was decreased to be 100 K, the saturation magnetizations were increased to be 28.10 emu/g, 17.72 emu/g and 2.96 emu/g for the samples prepared at the conditions of using 0.1 M, 0.05 M, and 0.01 M aqueous iron ion solutions, respectively (Figure 3.7b). The increasing of the saturation magnetization with the decreasing of temperature is a typical behavior of magnetic nanoparticles that resulted from the decreasing of thermal energy (Chen & Chen 2001). In comparison between step wised-dipping process and ammonia gas-enhancing *in situ* co-precipitation method at the same preparation condition using 0.05 M aqueous iron ion solution, the saturation magnetization of magnetic particle-incorporated bacterial cellulose membranes prepared by step wised-dipping process was reported to be 3.5 emu/g (Sourty, Ryan, & Marcessault, 1998) whereas the saturation magnetization of magnetic particle-incorporated bacterial cellulose prepared by ammonia gas-enhancing *in situ* co-precipitation method was 16 emu/g. The large difference in the saturation magnetization between the two preparation methods may result from the

difference in percentage loading of magnetic particles into bacterial cellulose matrix the difference in percent incorporation of magnetic particles into bacterial cellulose matrix. Weight percent of iron in the sample prepared by step wised-dipping process was 20.91% (Sourty, Ryan, & Marcessault, 1998) whereas weight percent of iron in the sample prepared by ammonia gas-enhancing *in situ* co-precipitation method was 47.21% as determined by EDX. The ammonia gas-enhancing *in situ* co-precipitation method accomplished the greater iron loading ability than the stepwise-dipping process. Regarding to ammonia gas-enhancing *in situ* co-precipitation method, the maximum saturation magnetization of the magnetic particle-incorporated bacterial cellulose sheet could be elevated to 26.20 emu/g. Guo *et al.* (2009) prepared electrospun poly(acrylonitrile-co-acrylic acid) nanofibrous composites containing 60 and 44 wt.% of magnetite nanoparticles (Fe_3O_4). The average particle size of the magnetite nanoparticles (Fe_3O_4) was 30 nm. The saturation magnetization of the electrospun poly(acrylonitrile-co-acrylic acid) nanofibrous composites containing magnetite (Fe_3O_4) was increased from 27.02 emu/g to 30.51 emu/g with increasing percentage loading of magnetite particles (Fe_3O_4) from 44 wt.% to 60 wt.%, respectively. According to the method of Ghule *et al.* (2006), the percent incorporation of magnetic particles in the as-prepared bacterial cellulose sheet was determined by using TGA. Table 1 shows the percent incorporation of magnetic particles in the magnetic particle-incorporated bacterial cellulose sheet prepared by ammonia gas-enhanced *in situ* co-precipitation method using 0.1 M, 0.05 M and 0.01 M aqueous iron ion solutions. When the concentrations of aqueous iron ion solutions were decreased from 0.1 M to 0.05 M and to 0.01 M, the percent incorporation of magnetic particles in the as-prepared samples decreased from 51.69% to 40.36% and to 20.37%, respectively. Therefore, the increasing of saturation magnetizations of the as-prepared magnetic particle-incorporated bacterial cellulose sheets with the increasing of the concentrations of aqueous iron ion solutions resulted from the higher amount of the incorporated magnetic particles in bacterial cellulose sheets. Not only the amount of magnetic particles but also the crystal structure of iron oxide affected the saturation magnetization. It is known that the magnetite particle exhibits the strongest magnetism of any transition metal oxides (Cornell & Schwertmann, 2003; Majewski & Thierry, 2007). According to Guardia *et al.* (2007), the saturation

magnetization of magnetic particle-incorporated composite did not depend on the particle size of magnetic particles but it depended on the amount of magnetic particles inside the matrix. Therefore, the requirements for achieving the appreciable magnetic properties are the high percentage loading of magnetic particles and the magnetic particles should be in the form of magnetite (Fe_3O_4). Both requirements could be achieved by using the ammonia gas-enhancing *in situ* co-precipitation method.

The magnified view of the hysteresis loops of the magnetic particle-incorporated bacterial cellulose sheet at 300 K and 100 K were shown in Figure 3.7c and 3.7d, respectively. When the concentration of aqueous iron ion solutions were decreased from 0.1 M to 0.05 M and to 0.01 M, the smaller hysteresis loop, the lower remnant magnetization (M_r) and the lower coercive field (H_c) were obtained. At the temperature of 300 K, the remnant magnetizations were found to be 2.67 emu/g, 1.42 emu/g, and 0.15 emu/g whereas the coercive fields were found to be 65 G, 40 G and 40 G for the samples prepared at the conditions of using 0.1 M, 0.05 M and 0.01 M aqueous iron ion solutions, respectively. Similar results were also reported in the studies of Guo *et al.* (2009) and Guardia *et al.* (2007). It might be concluded that the remnant magnetization and coercive field were decreased with decreasing the particle size of magnetic particles. In order to achieve the superparamagnetic behavior of magnetic particle-incorporated bacterial cellulose sheet, the remnant magnetization (M_r) and the coercive field (H_c) of the as-prepared sample should be as low as possible. By using ammonia gas-enhanced *in situ* co-precipitation method, the particle sizes of magnetic particles were ranged from 19.62 to 38.92 nm which is the lowest reported value of particle size in comparison with the other preparation methods (Sourty, Ryan, & Marcessault, 1998). The ammonia gas-enhanced *in situ* co-precipitation method is a promising method for preparing of the magnetically responsive bacterial cellulose. At the temperature of 100 K, the remnant magnetizations were found to be 8.43 emu/g, 5.32 emu/g and 0.52 emu/g whereas the coercive fields were found to be 120 G, 98 G and 49 G for the samples prepared at the conditions of using 0.1 M, 0.05 M and 0.01 M aqueous iron ion solutions, respectively. Regarding to these results, it was found that the remnant magnetization (M_r) and the coercive field (H_c) at the temperature of 100 K were significantly higher

than the values at the temperature of 300 K. The explanation might be lined on the magnetic relaxation time. For nanometer scaled-diameter of magnetic particles, the magnetic relaxation time was exponentially increased with decreasing of the temperature (Mcnab, Fox, & Boyle, 1986). At low temperature, when the applied field was reached to zero, the dipole moments of some nanoparticles were still polarized since it required a longer time for relaxing to be zero magnetization. Therefore, a small increment of the remnant magnetization and coercive field were observed at 100 K (Wang *et al.*, 2004).

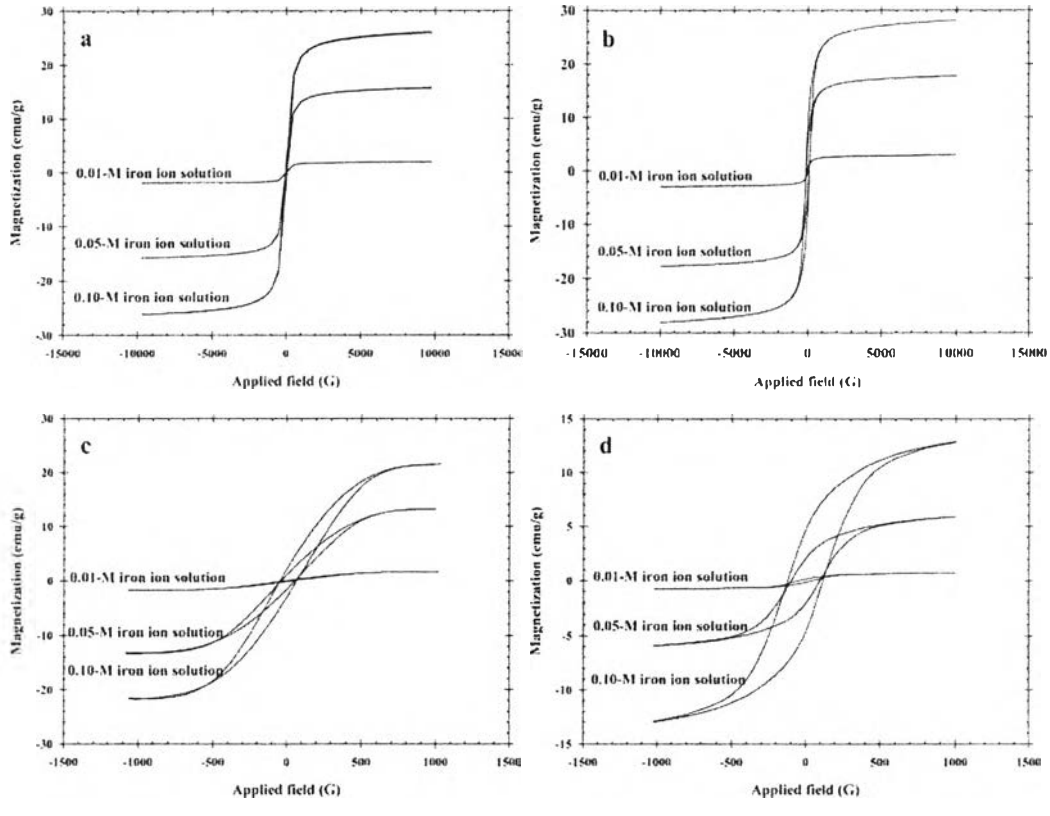

Figure 3.7 Magnetic hysteresis loop of magnetic particle-incorporated bacterial cellulose sheet at the temperature of 300 K (a) and 100 K (b) and magnified view of its hysteresis loop at the temperature of 300 K (c) and 100 K (d).

3.4.5 Magnetic field responsiveness testing

While applying a magnetic field, the magnetic particle-incorporated bacterial cellulose sheet was deformed by the translational forces experienced by the incorporated magnetic particles. The response of a strip of the freeze-dried magnetic particle-incorporated bacterial cellulose sheet to the magnetic field provided by a laboratory magnet with exhibited the magnetic field at 1000 tesla. One end of the magnetic particle-incorporated bacterial cellulose strip was fixed to an aluminum plate while the other end was free to move. Without the magnetic field, the magnetic particle-incorporated bacterial cellulose strip laid flat on the surface of the aluminum plate. When the magnetic field was applied, the magnetic particle-incorporated bacterial cellulose strip was deformed in the direction of increasing magnetic field. Wang *et al.* (2004) prepared nanocomposite of PEO/magnetite nonwoven mat and PVA/magnetite nonwoven mat by electrospinning technique. Both nonwoven mats were easily magnetized by an external magnetic field and deflected in the presence of the applied magnetic field. Table 1 showed the iron content and displacement responding to the external magnetic field of the magnetic particle-incorporated bacterial cellulose sheets. The respond of the magnetic particle-incorporated bacterial cellulose sheets to the external magnetic field were determined by the displacement distance (d) and the displacement angle (Θ). For, the sample synthesized by using 0.01 M aqueous iron ion solution, the displacement distance (d) and the displacement angle (Θ) were 2.7 cm and 28.6°, respectively (Table 1). When the concentrations of aqueous iron ion solution were increased from 0.01 M to 0.05 M and to 0.1 M, the displacement distance (d) and the displacement angle (Θ) were increased to be 5 cm and 53.9° and to be 6.3 cm and 62.7°, respectively (Table 1). The greater deflection of the magnetic particle-incorporated bacterial cellulose strip with increasing concentrations of aqueous iron ion solution resulted from the larger translational forces of the higher amount of the incorporated magnetic particles in the bacterial cellulose samples.

Table 3.1 The percent incorporation of magnetic particle, weight percent of iron content and displacement responding to the magnetic field of magnetic particle-incorporated bacterial cellulose sheet prepared by ammonia gas-enhanced *in situ* co-precipitation method using 0.1 M, 0.05 M, and 0.01 M aqueous iron ion solution

Concentration of aqueous iron ion solution (M)	Percent incorporation of magnetic particle (%)	Iron content (weight percent)	Displacement	
			Distance (cm)	Angle (degree)
0.01	20.37 ± 0.10	32.29	6.3	62.7
0.05	40.36 ± 1.01	47.12	5.0	53.9
0.1	51.69 ± 1.15	57.23	2.7	28.6

3.5 Conclusions

In this study, homogeneous dispersion of magnetic nanoparticles in bacterial cellulose matrix was achieved by using ammonia gas-enhancing *in situ* co-precipitation method operated in a closed system without oxygen. The use of ammonia gas, instead of conventional aqueous basic solutions, could prevent the accumulation of magnetic particles at the surface of bacterial cellulose, resulting in the homogeneous dispersion of the magnetic nanoparticles throughout the bacterial cellulose matrix. Accordingly, the as-prepared magnetic nanoparticles-incorporated bacterial cellulose sheet exhibited the uniform magnetic properties throughout the bacterial cellulose matrix. Moreover, the homogeneous dispersion of the magnetic nanoparticles throughout the bacterial cellulose matrix could the percent incorporation of magnetic nanoparticles into bacterial cellulose samples leading to high and uniform magnetic properties throughout the matrix of bacterial cellulose. Regarding to the uses of bacterial cellulose pellicle and ammonia gas-enhancing *in situ* co-precipitation method, magnetic particles in the crystal form of magnetite (Fe_3O_4) were obtained and the diameter of the as-synthesized magnetic particles were

ranged in the nanoscale. The average particle sizes of the magnetic nanoparticles were in the range of 20–39 nm. The particle size and particle size distribution of magnetic nanoparticles were controllable by adjusting the concentration of aqueous iron ion solution. The saturation magnetization of the magnetic nanoparticle-incorporated bacterial cellulose sheet ranged from 1.92 to 26.20 emu/g with very low remnant magnetization (0.15–2.67 emu/g) and coercive field (40–65 G) at the room temperature. Moreover, the responsiveness to an externally applied magnetic field of the magnetic nanoparticle-incorporated bacterial cellulose sheet was exhibited by its deflection in the direction of increasing magnetic field. All evidences reveal that the magnetically responsive bacterial cellulose sheet was successfully prepared by ammonia gas-enhancing *in situ* co-precipitation method. Moreover, the preparation method is simple and cost-effective, which may lead to the more development for new applications, such as microwave absorption devices and enzyme immobilization for biosensor applications. Not only for bacterial cellulose but this preparation method may be used to achieve magnetic properties in other materials such as electro-spun nanofiber mat and other porous materials.

3.6 Acknowledgements

Financial support from the Chulalongkorn University Dutsadi Phiphat Scholarship, the Rachadapisek Somphot Endowment Fund, the Petroleum and Petrochemical College, Chulalongkorn University, and the Center for Petroleum, Petrochemicals and Advanced Materials, Chulalongkorn University, Thailand, is greatly acknowledged.

3.7 References

Baker, C., Ismat Shah, S., & Hasanain S. K. (2004). Magnetic behavior of iron and iron-oxide nanoparticle/polymer composites. *Journal of Magnetism and Magnetic Materials, 280*, 412–418.

Chen, D., & Chen, Y. (2001). Synthesis of Barium Ferrite Ultrafine Particles by Coprecipitation in the Presence of Polyacrylic Acid. *Journal of Colloid and Interface Science, 235*, 9–14.

Cornell, R. M. & Schwertmann, U. (2003). *The Iron Oxides: Structure, Properties, Reactions, Occurrences and Uses.* (2nd ed.). Weinheim: Wiley-VCH.

Czaja, W. K., Romanovicz, D., & Brown, R. M. (2004). Structural investigations of microbial cellulose produced in stationary and agitated culture. *Cellulose, 11*, 403–411.

Czaja, W. K., Young, D. J., Kawecki, M., & Brown, R. M. (2007). The future prospects of microbial cellulose in biomedical applications. *Biomacromolecules, 8*, 1–12.

Deepa, T., Palkar, V. R., Kurup, M. B., & Malik S. K. (2004). Properties of magnetite nanoparticles synthesized through a novel chemical route. *Materials Letter, 58*, 2692–2694.

Dikeakos, M., Tung, L. D., Veres, T., Stancu, A., Spinu, L., & Normandin, F. (2003). Fabrication and characterization of tunable magnetic nanocomposite materials. *Materials Research Society Symposium Proceedings, 734*, 315–320.

Dubey, V., Saxena, C., Singh, L., Ramana, K. V., & Chauhan, R. S. (2002). Pervaporation of binary water–ethanol mixtures through bacterial cellulose membrane. *Separation and Purification Technology, 27*, 163–171.

Epstein, A. J., & Miller J. S. (1996). Molecule- and polymer-based magnets, a new frontier. *Synthetic Metals, 80*, 231–237.

Filipcsei, G., Csetneki, I., Szilágyi, A., & Zrínyi, M. (2007). Magnetic Field-Responsive Smart Polymer Composites. *Advances in Polymer Science, 206*, 137–189.

Ghule, K., Ghule, A. V., Chen B., & Ling, Y. (2006). Preparation and characterization of ZnO nanoparticles coated paper and its antibacterial activity study. *Green Chemistry, 8*, 1034–1041.

Green, H. V., Fox, T. J., & Scallan, A. M. (1982). Lumen loaded paper pulp. *Pulp and Paper Canada, 83(7)*, 203–207.

Guardia, P., Batlle-Brugal, B., Roca, A. G., Iglesias, O., Morales, M. P., Serna, C. J., Labarta, A., & Batlle X. (2007). Surfactant effects in magnetite nanoparticles of controlled size. *Journal of Magnetism and Magnetic Materials, 316*, 756–759.

Guo, J., Ye, X., Liu, W., Wu, Q., Shen, H., & Shu, k. (2009). Preparation and characterization of poly(acrylonitrile-co-acrylic acid) nanofibrous composites with Fe_3O_4 magnetic nanoparticles. *Materials Letters, 63*, 1326–1328.

Hu, W., Chen, S., Li, X., Shi, S., Shen, W., Zhang, X., & Wang, H. (2009). In situ synthesis of silver chloride nanoparticles into bacterial cellulose membranes. *Materials Science and Engineering C, 29*, 1216–1219.

Hu, W., Chen, S., Zhou, B., & Wang, H. (2010). Facile synthesis of ZnO nanoparticles based on bacterial cellulose. *Materials Science and Engineering B, 170*, 88–92.

Jiles, D. (1991). *Introduction to Magnetism and Magnetic Materials.* London: Chapman & Hall/CRC.

Kamel, S. (2007). Nanotechnology and its applications in lignocellulosic composites, a mini review. *eXPRESS Polymer Letters, 1*, 546–575.

Kim, J. S., Yoon, T. J., Yu, K. N., Kim, B. G., Park, S. J., Kim, H. W., Lee, K. H., Park, S. B., Lee, J. K., & Cho, M. H. (2005). Toxicity and tissue distribution of magnetic nanoparticlesin mice. *Journal of Toxicological Sciences, 89*, 338–347.

Li, X., Chen, S., Hu, W., Shi, S., Shen, W., Zhang, X., & Wang, H. (2009). *In situ* synthesis of CdS nanoparticles on bacterial cellulose nanofibers. *Carbohydrate Polymers, 76*, 509–512.

Marchessault, R. H., Richard, S., & Rioux, P. (1992). In situ synthesis of ferrites in lignocellulosics. *Carbohydrate Research, 224*, 133–139.

Marchessault, R. H., Rioux, P., & Raymond, L. (1992). Magnetic cellulose fibers and paper: preparation, Processing and properties. *Polymer, 33(19)*, 4024–4028.

Majewski, P., Thierry, B. (2007). Functionalized magnetite nanoparticles–synthesis, properties, and bio-applications. *Critical Reviews in Solid State and Materials Science, 32*, 203–215.

Maneerung, T., Tokura, S., & Rujiravanit, R. (2008). Impregnation of silver nanoparticles into bacterial cellulose for antimicrobial wound dressing. *Carbohydrate Polymers, 72*, 43–51.

McNab, T. K., Fox, R. A., & Boyle, A. J. F. (1986) Some Magnetic Properties of Magnetite (Fe_3O_4) Microcrystals. *Journal of Applied Physics, 39*, 5703–5711.

Meftahi, A., Khajavi, R., Rashidi, A., Sattari, M., Yazdanshenas, M. E., & Torabi, M. (2010). The effects of cotton gauze coating with microbial cellulose. *Cellulose, 17*, 199–204.

Neuberger, T., Schopf, B., Hofmann, H., Hofmann, M., & Rechenberg, B. (2005). Superparamagnetic nanoparticles for biomedical applications: Possibilities and limitations of a new drug delivery system. *Journal of Magnetism and Magnetic Materials, 293*, 483–496.

Passaretti, J. D., Caulfield, D. F. & Sobczynski, S. F. (1990). Materials Interactions Relevant to the Pulp, Paper and Wood Industries. *Materials Research Society, 197 (pp. 319)*. San francisco, California.

Pinchuk, L. S., Markova, L. V., Gromyko, Y. V., Markov, E. M., & Choi, U. S. (1995). Polymeric magnetic fibrous filters. *Journal of Materials Processing Technology, 55*, 345–350.

Raymond, L., Revol, J. F., Ryan, D. H., & Marchessault, R. H. (1994). *In situ* synthesis of ferrites in cellulosics. *Chemistry of Material, 6*, 249–255.

Rioux, P., Ricard, S., & Marchessault, R. H. (1992). The preparation of magnetic papermaking fibres. *Journal of Pulp and Paper Science, 18(1)*, 39–43.

Rodriguez-Fernandez, O. S., Rodriguez-Calzadiaz, C. A, Yanez-Flores, I. G., & Montemayor, S. M. (2008). Preparation and characterization of a magneto-polymeric nanocomposite: Fe_3O_4 nanoparticles in a grafted, cross-linked and plasticized poly(vinyl chloride) matrix. *Journal of Magnetism and Magnetic Materials, 320*, e81–e84.

Shchukin, D. G., Radtchenko, I. L., & Sukhorukov, G. B. (2003). Micron-scale hollow polyelectrolyte capsules with nanosized magnetic Fe3O4 inside. *Materials Letters, 57*, 1743–1747.

Small, A. C., & Johnston, J. H. (2009). Novel hybrid materials of magnetic nanoparticles and cellulose fibers. *Journal of Colloid and Interface Science, 331*, 122–126.

Sourty, E., Ryan, D. H., & Marchessault, R. H. (1998). Characterization of magnetic membranes based on bacterial and man-made cellulose. *Cellulose, 5*, 5–17.

Starodoubtsev, S. G., Saenko, E. V., Khokhlov, A. R., Volkov, V. V., Dembo, K. A., Klechkovskaya,V. V., Shtykova, E. V., & Zanaveskina, I. S. (2003). Poly(acrylamide) gels with embedded magnetite nanoparticles. *Microelectronic Engineering, 69*, 324–329.

Tartaj, P., Morales, M. P., Gonzalez-Carreno, T., Veintemillas-Verdaguer, S., & Serna, C. J. (2005). Advances in magnetic nanoparticles for biotechnology applications. *Journal of Magnetism and Magnetic Materials, 290–291*, 28–34.

Tartaj, P., Morales, M. D., Veintemillas-Verdaguer, S., Gonzalez-Carreno, T., & Serna, C. J. (2003). The preparation of magnetic nanoparticles for applications in biomedicine. *Journal of Physics D: Applied Physics, 36*, R182–R197.

Teja, A. S., & Koh, P. (2009). Synthesis, properties, and applications of magnetic iron oxide nanoparticles. *Progress in Crystal Growth and Characterization of Materials, 55*, 22–45.

Wang, M., Singh, H., Hatton, T. A., & Rutledge, G. C. (2004). Field-responsive superparamagnetic composite nanofibers by electrospinning. *Polymer, 45*, 5505–5514.

Zhang, D., & Qi, L. (2005). Synthesis of mesoporous titania networks consisting of anatase nanowires by templating of bacterial cellulose membranes. *Chemical Communications, 21*, 2735–2737.